

# Linking star formation thresholds and truncations in the thin and thick disks of the low-mass galaxy UGC 7321

S. Díaz-García<sup>1,2,3,4</sup>, S. Comerón<sup>2,1</sup>, S. Courteau<sup>3</sup>, A. E. Watkins<sup>5</sup>, J. H. Knapen<sup>1,2</sup>, and J. Román<sup>1,2,6</sup>

<sup>1</sup> Instituto de Astrofísica de Canarias, E-38205, La Laguna, Tenerife, Spain  
e-mail: simondiazgar@gmail.com

<sup>2</sup> Departamento de Astrofísica, Universidad de La Laguna, E-38205, La Laguna, Tenerife, Spain

<sup>3</sup> Department of Physics, Engineering Physics & Astrophysics, Queen's University, Kingston, ON K7L 3N6, Canada

<sup>4</sup> Personal Docente, Consejería de Educación, Universidades, Cultura y Deportes del Gobierno de Canarias, E-35002, Las Palmas de Gran Canaria, Spain

<sup>5</sup> Centre for Astrophysics Research, School of Physics, Astronomy and Mathematics, University of Hertfordshire, Hatfield AL10 9AB, UK

<sup>6</sup> Kapteyn Astronomical Institute, University of Groningen, PO Box 800, 9700 AV Groningen, The Netherlands

Received 14 October 2021; accepted 29 August 2022

## ABSTRACT

Thin and thick disks are found in most spiral galaxies, yet their formation scenarios remain uncertain. Whether thick disks form through slow or fast, internal or environmental, processes is unclear. The physical origin of outer truncations in thin and thick disks, observed as a drop in optical and near-infrared (NIR) surface brightness profiles, is also a much debated topic. These truncations have been linked to star formation (SF) thresholds in Milky-Way-type galaxies, but no such connection has been made for their low-mass counterparts or in thick disks. Our photometric analysis of the edge-on galaxy UGC 7321 offers a possible breakthrough. This well-studied diffuse, isolated, bulgeless, ultra-thin galaxy is thought to be under-evolved both dynamically and in SF. It is an ideal target for disentangling internal effects in the formation of thick disks and truncations. Our axial light profiles from deep far- and near-ultraviolet (GALEX) images, tracing recent SF, and optical (DESI *grz*) and NIR (*Spitzer* 3.6  $\mu\text{m}$ ) images, tracing old stellar populations, enable a detailed identification of an outer truncation in all probed wavelengths in both the thin and thick disks. After deprojecting to a face-on view, a sharp truncation signature is found at a stellar density of  $1.5 \pm 0.5 \mathcal{M}_{\odot} \text{pc}^{-2}$ , in agreement with theoretical expectations of gas density SF thresholds. The redder colours beyond the truncation radius are indicative of stellar migration towards the outer regions. We thus show that thick disks and truncations can form via internal mechanisms alone, given the pristine nature of UGC 7321. We report the discovery of a truncation at and above the mid-plane of a diffuse galaxy that is linked to a SF threshold; this poses a constraint on physically motivated disk size measurements among low-mass galaxies.

**Key words.** galaxies: individual UGC 7321 - galaxies: structure - galaxies: star formation

## 1. Introduction

The presence of sharp drops in the outer parts of the surface brightness (SB) profiles of some edge-on galaxies has been known for decades (Freeman 1970; van der Kruit 1979). The formation of these so-called truncations has been studied extensively in galaxies of different inclinations (e.g. Pohlen & Trujillo 2006; Foyle et al. 2008; Roediger et al. 2012; Comerón et al. 2012; Fliri & Trujillo 2016) and redshifts ( $z$ ; e.g. Pérez 2004).

Truncations have been linked to a critical gas surface density for star formation (SF; Martin & Kennicutt 2001). Examples include the Milky Way (MW)-like edge-on galaxies NGC 4565 and NGC 5907, whose large angular sizes allow for a photometric analysis with high spatial resolution. Martínez-Lombilla et al. (2019) identified truncations in their disks, at heights of up to  $\sim 3$  kpc, from near-ultraviolet (NUV; tracer of recent SF), optical (stacked *gri*), and near-infrared (NIR; 3.6  $\mu\text{m}$ , tracer of old stellar populations) wavelengths. Truncations in these two galaxies lie at a stellar surface density ( $\Sigma_{\star}$ ) of  $\sim 1 - 2 \mathcal{M}_{\odot} \text{pc}^{-2}$  (Martínez-Lombilla et al. 2019), which is consistent with the critical gas surface density ( $\sim 3 - 10 \mathcal{M}_{\odot} \text{pc}^{-2}$ ) beyond which gas can no longer be transformed into stars (Schaye 2004). In this paper we extend this work into the realm of low-mass galaxies with

an analysis of the truncated diffuse edge-on galaxy UGC 7321 (maximum circular velocity  $V_c = 108 \text{ km s}^{-1}$ ; Springob et al. 2005).

Chamba et al. (2020) and Trujillo et al. (2020) proposed the radius corresponding to the isomass contour at  $1 \mathcal{M}_{\odot} \text{pc}^{-2}$  as a physically motivated disk size measurement ( $R_1$ ) for face-on and moderately inclined galaxies. This is supported by the aforementioned  $\Sigma_{\star}$  values at the truncation of MW-type galaxies. The use of  $R_1$  yields a narrower stellar mass–size relation than the half-light radius (see also Sánchez Almeida 2020; Arora et al. 2021; Watkins et al. 2022). Similar conclusions were reached by Muñoz-Mateos et al. (2015) using the 25.5 mag arcsec<sup>-2</sup> isophotal radius from 3.6  $\mu\text{m}$  images from the *Spitzer* Survey of Stellar Structure in Galaxies (S<sup>4</sup>G; Sheth et al. 2010). Below, we study  $\Sigma_{\star}$  at the edge of a low-mass low-SB galaxy to further constrain its size.

Thick disks — the faint, large scale-height counterpart of thin discs — are frequently identified in edge-on galaxies and can also present truncations (e.g. Comerón et al. 2011). They are dominant in low-mass galaxies (Yoachim & Dalcanton 2006). Their formation, whether fast or slow, internal or driven by the environment, is also a point of contention. Thick disks could be

the fossil record of a primordial turbulent disk (e.g. Elmegreen & Elmegreen 2006) built through an intense SF episode (Comerón et al. 2014) or quickly formed at high  $z$  through wet mergers (e.g. Brook et al. 2004). They could also gradually arise from stars stripped from, and dynamically heated by, infalling satellites (Abadi et al. 2003) or via internal mechanisms such as radial migration (Schönrich & Binney 2009) and dynamical heating by giant molecular clouds (Villumsen 1985). Thick disk formation can result from the simultaneous interplay of internal and external processes (Minchev et al. 2015; Pinna et al. 2019), though we now focus on the former by studying a galaxy (UGC 7321) without a strong sign of environmental activity.

UGC 7321 is catalogued as an isolated galaxy by Verdes-Montenegro et al. (2005) and Henkel et al. (2017). NGC 4204 appears at an offset of  $\approx 2^\circ$  southwards, and NGC 4455 lies at an even larger angular distance, though both galaxies are a factor of  $\sim 2$  closer to us than UGC 7321 (e.g. Karachentsev et al. 2006; Nasonova et al. 2011; Henkel et al. 2017). The isolation of UGC 7321 is further confirmed from the low values of the projected surface density to the third nearest neighbour ( $\Sigma_3^A = 0.7$ ) and its Dahari parameter ( $Q = -5.1$ ) (Dahari 1984) in a velocity interval of  $\pm 500 \text{ km s}^{-1}$ , following Laine et al. (2014). Inspection of optical images from the Dark Energy Spectroscopic Instrument (DESI) Legacy Imaging Surveys (Dey et al. 2019) does not reveal the presence of any low-SB satellite within an area encompassing a factor of several times the galaxy radius, down to depths of  $\mu_g(\text{AB}) = 28.9 \text{ mag arcsec}^{-2}$  and  $\mu_r(\text{AB}) = 28.2 \text{ mag arcsec}^{-2}$  ( $3\sigma$ ,  $10'' \times 10''$  boxes; Román et al. 2020). Hence, the main photometric and kinematic properties of UGC 7321 are likely not affected or caused by interactions. The presence of extremely faint dwarfs cannot be discarded, as their detection might demand even deeper imaging (see e.g. Henkel et al. 2017).

UGC 7321 is also a bulgeless galaxy with a very cold disk (Matthews et al. 1999), hinting at a quiescent merger history (Sarkar & Jog 2019). However, its warped H I disk is indicative of a possible encounter ( $> 1.6 \text{ Gyr}$  ago) with a neighbour, followed by disk cooling (Uson & Matthews 2003), or angular momentum misalignments between the disk and the dark matter halo (Debattista & Sellwood 1999). Such a warp could indeed be of intrinsic origin (see further discussion in Bosma 2017). UGC 7321's ultra-thin disk (Bizyaev et al. 2017) suggests a higher spin parameter than those of low-SB and regular disk galaxies (Jadhav Y & Banerjee 2019) or a dark matter dominance (Banerjee & Jog 2013). Also, ultra-thin galaxies have been found in specific cosmic web environments with a very low density, as they are less connected with filaments (Bizyaev et al. 2017). Altogether, UGC 7321 appears to be extremely isolated and under-evolved in terms of dynamics and SF (e.g. Matthews et al. 1999).

UGC 7321 has a thick disk. Early studies of its vertical density distribution revealed that a single  $\text{sech}^{2/n}$  fit cannot reproduce optical observations; a second component is needed (Matthews 2000). The model of Sarkar & Jog (2019) – including a gravitationally coupled stellar disk and a H I disk in the potential of a dark matter halo (see also Banerjee et al. 2010) – suggests that  $n$  cannot be trusted as a robust parameter, as it varies with radius and fitting range, and thus a double-disk fit may not be necessary. This model is, on the other hand, based on the relatively shallow optical surface photometry from Matthews et al. (1999). Even so, a thick disk was already detected in the Matthews et al.  $B-R$  colour maps. The deeper  $3.6 \mu\text{m}$  imaging from the S<sup>4</sup>G and distance-independent photometric decomposition models of Comerón et al. (2018) confirm that a thick disk is definitely needed to fit the vertical SB profiles (see their Appendix B). Comerón et al. assumed fitting functions for two stel-

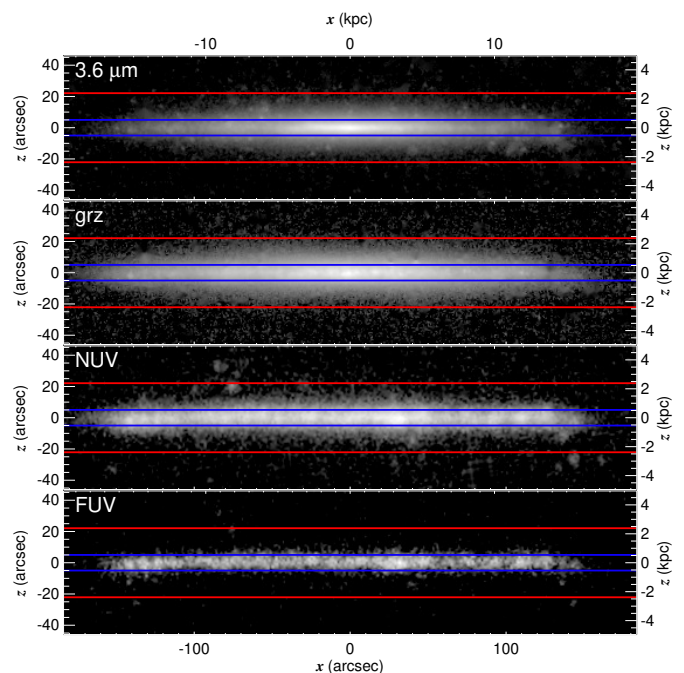


**Fig. 1.** From top to bottom, rotated sky-subtracted images of the low-mass ultra-thin galaxy UGC 7321 in  $3.6 \mu\text{m}$ ,  $grz$  (stacked), NUV, and FUV. The red lines indicate the height at which SB equals  $26 \text{ mag arcsec}^{-2}$  in  $3.6 \mu\text{m}$ , while the blue lines show the height ( $5''$ ) above which 90% of the light comes from the thick disk. These values are averaged from the vertical luminosity cuts of Comerón et al. (2018).

lar disks and one gaseous isothermal coupled disk in equilibrium, and their fit is used in this article.

In addition, a truncation in both the thin and thick disks is detected in the  $3.6 \mu\text{m}$  SB axial<sup>1</sup> profiles by Comerón et al. (2018). Here, we revisit this truncation in NUV, far-ultraviolet (FUV),  $grz$ , and  $3.6 \mu\text{m}$  NIR images of UGC 7321 in order to study its connection to SF thresholds. Such a connection found in thick disks would constrain formation scenarios, given their expected old age. For comparison with MW-type galaxies, the SB profiles of NGC 4565 ( $V_c = 250 \text{ km s}^{-1}$ ; Springob et al. 2005) are also revisited; further details are available in Martínez-Lombilla et al. (2019) and Martínez-Lombilla et al. (in prep.). We adopt redshift-independent distances of  $22.28 \pm 3.34$  and  $13.43 \pm 2.01 \text{ Mpc}$  for UGC 7321 and NGC 4565, respectively (Tully et al. 2016), assuming a 15% uncertainty (Muñoz-Mateos et al. 2015).

## 2. Ultraviolet, optical, and near-infrared imaging

To trace old stellar populations (Courteau et al. 2014; Roediger & Courteau 2015), we used  $3.6 \mu\text{m}$  images from the S<sup>4</sup>G obtained with the Infrared Array Camera (Fazio et al. 2004) on board the *Spitzer* Space Telescope (Werner et al. 2004), with an exposure time of 240 s per galaxy. We also used stacked DESI  $g$ ,  $r$ , and  $z$  images, with nominal exposure times of 166, 134, and 200 s, respectively (Dey et al. 2019).

We probed recent SF with the Galaxy Evolution Explorer (GALEX) ultraviolet (UV) images from the catalogue of Bouquin et al. (2018). Specifically, we used NUV ( $\lambda_{\text{eff}} = 2267 \text{ \AA}$ ) and FUV ( $\lambda_{\text{eff}} = 1516 \text{ \AA}$ ) images with long exposure times: for UGC 7321, 1683 and 2822 s in FUV and NUV, respectively; for NGC 4565, 1693 s for both. The FUV emission traces

<sup>1</sup> The axial direction is the mid-plane projection of a vector pointing away from the galaxy centre in the sky plane.

SF of several tens to 100 Myr, while the NUV traces  $\lesssim 300$  Myr populations (Kennicutt 1998).

All images used the masks created by Comerón et al. (2018), and fluxes in masked regions were interpolated following Salo et al. (2015). The sky levels were measured within the same  $30'' \times 30''$  boxes as in Salo et al. (2015), which are located far from the galaxy. The median of the median values of each box was then subtracted from the images.

### 3. Axial surface-brightness profiles

The GALEX, DESI, and S<sup>4</sup>G images were aligned with the Interactive Data Language (IDL) package *hastrom*, which builds on the *poly\_2d* function to perform polynomial warping of images. The  $3.6 \mu\text{m}$  images were used as reference to match the astrometry. We then obtained axial SB profiles from the  $3.6 \mu\text{m}$ , *grz*, FUV, and NUV images (Fig. 1) by folding the images with respect to the mid-plane and averaging the flux between heights  $z = 0$  and  $z = z_u$ , where  $z_u$  is the height at which  $\mu_{3.6\mu\text{m}}(\text{AB}) = 26 \text{ mag arcsec}^{-2}$  on average. The latter was measured from vertical SB profiles presented in Comerón et al. (2018). The resulting SB values are sensitive to the selection of  $z_u$  — which was chosen to maximise the disk light and minimise the background noise — and are only used for the detection of the truncations. The axial profiles were then converted to face-on radial profiles (Sect. 3.2).

Following Pohlen & Trujillo (2006), we used a logarithmic binning in the axial direction: each range is 1.03 times wider than the previous, where the first data point is located at the S<sup>4</sup>G pixel size ( $0.75''$ ). Surface brightness profiles were folded with respect to the galaxy minor axis and averaged in the axial direction (asymmetries are discussed in Sect. 3.1). Vertical  $3.6 \mu\text{m}$  SB profiles were decomposed by Comerón et al. (2018) into thin and thick disks. As in their work, we hereafter consider the thin (thick) disk as the region below (above) the height at which 90% of the light comes from the thick disc (blue lines in Fig. 1).

A characterisation of the point spread function (PSF) may be required to reveal the faintest stellar structures (Peters et al. 2017; Martínez-Lombilla & Knapen 2019; Infante-Sainz et al. 2020; Román et al. 2020). We did not consider PSF modeling in NIR and optical wavelengths, however, as we are not probing the dimmest regions of thick disks ( $> 26 \text{ mag arcsec}^{-2}$ ) in vertical SB profiles, where PSF effects become dominant (see e.g. Comerón et al. 2018; Martínez-Lombilla et al. 2019).

In order to assess whether the high-altitude UV emission in UGC 7321 can be caused by scattered light, we estimated the line PSF (LSF) following Elmegreen et al. (2017) (see also Verstappen et al. 2013). We used the GALEX NUV and FUV PSF, extended with a power law using the parametrisation by Hodges-Kluck et al. (2016). We compared the LSFs to vertically integrated SB profiles calculated from the inner  $30''$  and confirmed that the LSF is much narrower than the UV disk of UGC 7321. We then convolved the LSF with a  $\text{sech}^2$  disk with an exponential scale height of  $1.5''$  (Comerón et al. 2018) and found negligible differences relative to the LSF. We finally verified that the differences between a radial cut of the PSF and the LSF arise in the wings. The wings start affecting the LSF at  $\sim 1/100$  of the peak value, which is below our detection threshold. We thus conclude that the scattered UV light from PSF wings is limited to fainter SB levels than those probed in this work.

The outer truncations and their radii were identified using the break-finding algorithm of Watkins et al. (2019). Their method looks for significant changes in the mean of the local slope of the SB profile — obtained following Pohlen & Trujillo (2006) — using a cumulative sum (CS) of the difference from the mean.

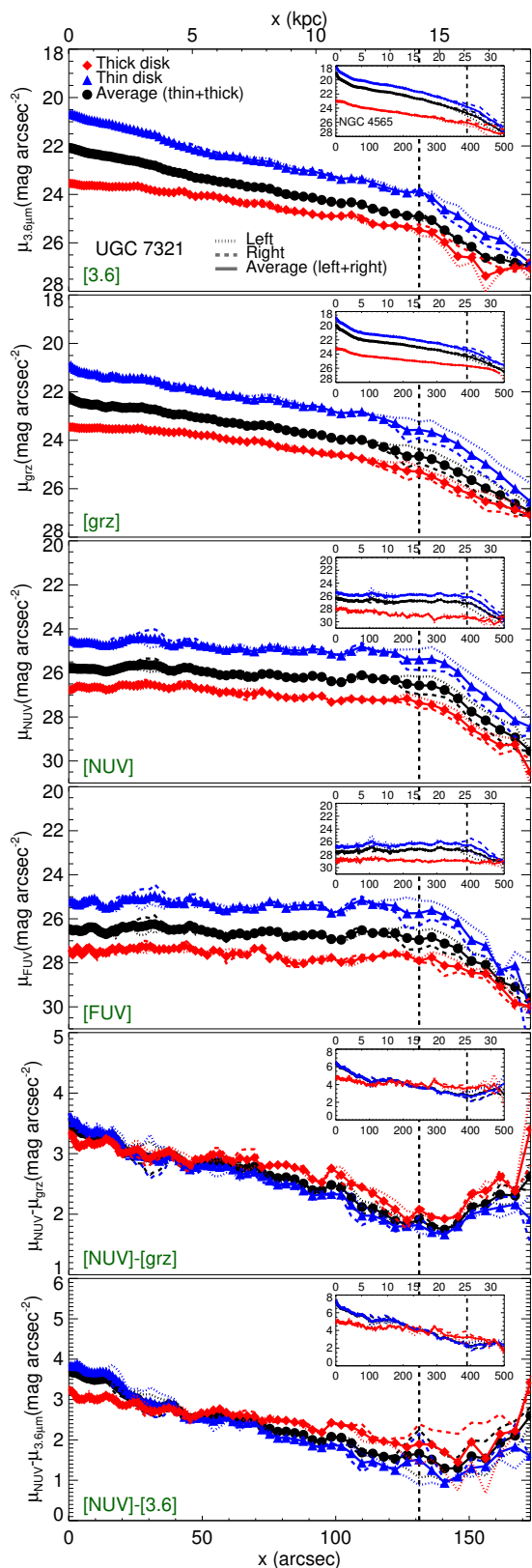


**Fig. 2.** Axial SB profiles of UGC 7321 at  $3.6 \mu\text{m}$  (first panel), *grz* combined mean (second panel), NUV (third panel), and FUV (fourth panel), along with the NUV-[*grz*] (fifth panel) and the NUV-[3.6] (sixth panel) colours. The radial profiles are shown for the thin disk (in blue), the thick disk (in red), and the entire disk (black). For consistency with Comerón et al. (2018), the analysis is limited to their outermost fitted point. The inset plots display the same radial profiles for the MW-type NGC 4565 (see also Martínez-Lombilla et al. 2019). The vertical dashed lines indicate the truncation loci in the  $3.6 \mu\text{m}$  images.

The location of the truncation corresponds to the maximum of the CS. The significance of the truncation is tested by bootstrapping the SB profile  $10^5$  times so that it is randomly reordered in the axial direction. The break strength — measured as  $\max(\text{CS}) - \min(\text{CS})$  — in the reordered profiles must also fall below that of the real profile in  $> 95\%$  of cases.

### 3.1. The NIR, optical, and UV truncations of UGC 7321

The SB profiles of UGC 7321 have the same outer truncation radius of  $131.3''$  or  $14.2 \pm 2.1$  kpc (Fig. 2) at all probed wavelengths (NUV, FUV, stacked *grz*,  $3.6 \mu\text{m}$ ). Likewise, we confirmed that truncations hold, at the same radii, in  $3.4 \mu\text{m}$  images from the Wide-field Infrared Survey Explorer (WISE; Jarrett et al. 2011) (Prof. T. Jarrett; private communication). We verified that the multi- $\lambda$  truncation is not due to a morphological asymmetry: it holds if, instead of symmetrising the axial profiles, we study separately the left and right sides along the major axis, as displayed in Fig. 1. This is not the case for NGC 4565 (Martínez-Lombilla et al. 2019; Gilhuly et al. 2020), which, unlike UGC 7321, is known to be interacting (e.g. Zschaechner et al. 2012).

The truncation in UGC 7321 appears at the same radius in both the thin and thick disks. (Since the latter are defined from  $3.6 \mu\text{m}$  SB decomposition models alone, the claim for the existence of a truncated thick disk with UV emission sources cannot be formally made; see Sect. 4.2.) Dust obscuration in the mid-plane is substantial in the UV (and milder in the NIR), but correcting for the dust is non-trivial and beyond the scope of this paper. As truncations were also identified above the mid-plane at all probed wavelengths, where there is less dust, they cannot be artificially created by dust obscuration (for a related discussion on the case of NGC 4565, see Martínez-Lombilla et al. 2019). Conversely, the dust distribution in galaxies with  $V_c < 120 \text{ km s}^{-1}$  is thought to have a larger scale-height and to be more diffuse than in their massive counterparts (Dalcanton et al. 2004). Nonetheless, it is known that UGC 7321 is not optically thick and that its internal extinction is low (Matthews et al. 1999). Also, the observed central UV SB is  $> 8$  mag dimmer than expected from an extrapolation of the observed SB profile slope beyond the truncation; such a difference cannot be solely ascribed to dust.

NUV-[3.6] and NUV-[*grz*] colours trace the specific SF rate (e.g. Bouquin et al. 2018), or the ratio of the SF rate to stellar mass surface densities, which in turn is related to the star formation efficiency (SFE; e.g. Saintonge et al. 2011). Colours become redder beyond the truncation of UGC 7321 (bottom two panels of Fig. 2; see Sect. 4 for a follow-up discussion).

### 3.2. Deprojection of the stellar surface density profiles

The SB of a highly inclined galaxy is enhanced due to line-of-sight integration of stars. Correcting for this effect is necessary for the photometric analysis of galaxies (e.g. Byun et al. 1994; Trujillo et al. 2020; Stone et al. 2021). Indeed, to expand the connection between SF thresholds and galaxy edges in low-mass galaxies, the stellar surface density at the truncation radius must be computed from deprojected NIR SB profiles.

The conversion of axial  $3.6 \mu\text{m}$  SB profiles ( $\mu_{3.6\mu\text{m}}$ ) to face-on radial profiles was done following Comerón et al. (2012). In short, broken disks are parametrised in the plane of the galaxy through the generalisation of broken exponential functions (Erwin et al. 2008) that are integrated along the line-of-sight. Figure 3 shows the 1D model of  $\mu_{3.6\mu\text{m}}$  for UGC 7321, as well as the

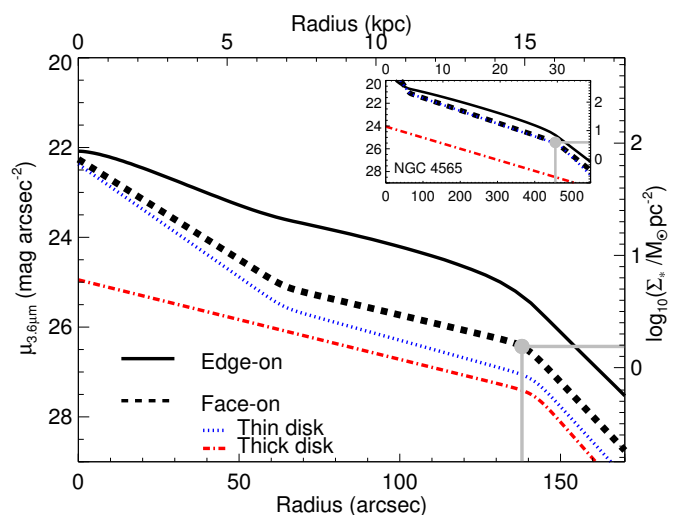


**Fig. 3.** 1D model of the  $3.6 \mu\text{m}$  axial SB profiles of UGC 7321 in edge-on (solid black line) and face-on (dashed black line) views. Blue (dotted) and red (dash-dotted) lines correspond to the deprojected radial profiles for the thin and thick disks, respectively. The right y axis displays the conversion to surface stellar densities. Vertical and horizontal grey lines highlight the y and x intercepts (in the galactic plane) at the truncation. The inset shows the same profiles for NGC 4565.

deprojected SB radial profiles for the thin and thick disks. For comparison, the insets display the same profiles for NGC 4565.

After deprojection, the multi-band truncation in UGC 7321 was identified at  $\mu_{3.6\mu\text{m}}(\text{AB}) \approx 26 \text{ mag arcsec}^{-2}$ , which is close to the SB limit of the S<sup>4</sup>G. This means that the survey is not ideally suited for the analysis of truncations in face-on galaxies, but sufficiently deep for their identification in edge-on galaxies. Deprojected  $3.6 \mu\text{m}$  SB profiles were converted to surface stellar densities ( $\Sigma_\star$ ) following Muñoz-Mateos et al. (2013):

$$\log_{10}(\Sigma_\star / [\mathcal{M}_\odot \text{ kpc}^{-2}]) = 16.76 - 0.4 \cdot \mu_{3.6\mu\text{m}} / [\text{mag arcsec}^{-2}], \quad (1)$$

adopting a stellar mass-to-light ratio  $\mathcal{M}_\star/L = \Upsilon_{3.6\mu\text{m}} = 0.53$  (Eskew et al. 2012). A 30% uncertainty on  $\mathcal{M}_\star/L$  was assumed (see Meidt et al. 2012).

The deprojected stellar density of UGC 7321 at the truncation is  $1.5 \pm 0.5 \mathcal{M}_\odot \text{ pc}^{-2}$  (grey lines in Fig. 3). In NGC 4565, the truncation occurs at  $3.9 \pm 1.2 \mathcal{M}_\odot \text{ pc}^{-2}$ , which is slightly larger than the  $\Sigma_\star$  ( $\sim 1 \mathcal{M}_\odot \text{ pc}^{-2}$ ) implied by Martínez-Lombilla et al. (2019) and Trujillo et al. (2020). This discrepancy, and the relevance of the local value of  $\Sigma_\star$  at the truncation, are discussed in Sect. 4.

## 4. Discussion

### 4.1. Galaxy sizes measured from SF thresholds

Many galaxies show SB truncations in their outskirts (e.g. Freeman 1970; van der Kruit 1979) at optical and NIR wavelengths. These have either been linked to the maximum angular momentum of the protogalactic cloud (e.g. van der Kruit 1987; Martín-Navarro et al. 2012) and the presence of disk warps (van der Kruit 1987) or to the presence of a SF threshold (Kennicutt 1989). Following the work of Martín & Kennicutt (2001), Trujillo et al. (2020) proposed exploring truncations in H $\alpha$  and UV to further constrain the link between galaxy edges and SF thresholds. This is tested here using deep UV, optical, and NIR imaging.

The isomass contour at  $1 \mathcal{M}_\odot \text{pc}^{-2}$  has been proposed as a proxy of the galaxy edge linked to a SF threshold (Chamba et al. 2020; Trujillo et al. 2020) (Sect. 1). We revisited this in two widely studied nearby edge-on galaxies, a MW-type and a low-mass diffuse galaxy, with a factor of 2.3 difference in  $V_c$ . Their disk truncations are found, in face-on view, at surface stellar densities of  $3.9 \pm 1.2$  and  $1.5 \pm 0.5 \mathcal{M}_\odot \text{pc}^{-2}$ , respectively. Trujillo et al. (2020) speculated that the gas density threshold for SF is lower in dwarf galaxies than in their more massive counterparts, possibly due to a lower SFE in low-mass galaxies (Leroy et al. 2008). This is in agreement with our observations.

We also report the existence of a NUV-[3.6] and NUV-[grz] colour upturn beyond the truncation in UGC 7321, in both the thin and thick disks (Sect. 3.1). A similar reddening was found in the NUV-[gri] colour profile of the thin disk of NGC 4565 (Martínez-Lombilla et al. 2019). These  $U$ -shaped profiles could be related to trends reported in previous works for low-inclination galaxies using optical colours (e.g. Bakos et al. 2008; Azzollini et al. 2008). They may indicate that the truncation is linked to a drop in SFE, but accurately probing the cold gas and properly correcting for dust would be needed for a decisive interpretation. In addition, Uson & Matthews (2003) argue that the  $\text{H I}$  gas surface density in UGC 7321 is systematically below that required for efficient SF based on the dynamical criterion of Kennicutt (1989). Deriving deprojected SFE profiles for edge-on galaxies is highly non-trivial. This effort might demand integral field unit data, which would also allow for the recovery of SF histories, which is beyond the scope of this paper.

We conclude that  $R_1$  is an accurate proxy of the disk size of UGC 7321. However, notable uncertainties are inherent to the deprojection of  $\Sigma_*$  and hence affect its local value at the truncation. The calibration of  $\mathcal{M}_*/L$  is non-trivial and can vary for galaxies of different masses and metallicities (e.g. Hall et al. 2018). Also, the scale height may vary with radius (see further discussion in Sect. 4.2). On the other hand, the radius of UGC 7321 is not necessarily representative of other galaxies of similar mass: ultra-thin galaxies have been claimed to have larger scale-lengths than ordinary disk galaxies given their higher stellar specific angular momentum (Jadhav Y & Banerjee 2019). While  $R_1$  can be used as a disk size definition in massive and faint galaxies, it is likely that the value of  $\Sigma_*$  at the disk edge is not constant for all masses.

#### 4.2. Thick disks can form through internal processes only

Whether thick disks form through internal or external, slow or fast, processes is still debated (Sect. 1). The analysis of UGC 7321 allows us to focus on internal slow processes alone, as this galaxy is isolated, bulgeless, and shows no clear signs of environmental activity at the explored SB levels (Sect. 1 and references therein). The relevant internal processes proposed include in situ thick disk formation, concomitant with the buildup of the galaxy, or secular heating and the radial migration of stars.

Thick disks truncate less frequently than thin disks (Comerón et al. 2011). When they do, the truncation radius is comparable to that in the thin disk. de Jong et al. (2007) reported that the truncation in the low-mass edge-on galaxy NGC 4244 occurs at the same radius for young, intermediate age, and old stars, at different heights above the mid-plane (up to 1.5 kpc). Based on the analysis of resolved stellar populations, Radburn-Smith et al. (2012) also concluded that the thin and the thick disk truncate at the same radius in the face-on spiral galaxy NGC 7793. These observational analyses led to the conclusion that dynamical processes are likely responsible for the occurrence of truncations in

both thin and thick disks, while SF thresholds were discarded as an explanation for this phenomenon (e.g. de Jong et al. 2007). If this were indeed the case, the different formation epochs of the two components should place their truncations at different radii.

Interestingly, Martínez-Lombilla et al. (2019) find truncations at and above the mid-plane (up to 3 kpc) at the same radius in NUV, *gri*, and  $3.6 \mu\text{m}$  images in two MW-like galaxies; these truncations are compatible with a SF threshold. NGC 4565's multi- $\lambda$  truncation is, however, not found in SB axial profiles averaged over the thick disk (Sect. 3.1). This is expected, as massive galaxies likely formed their thick disk  $\sim 8 - 10$  Gyr ago (Comerón 2021). Signatures of a SF threshold in the thick disk could have been washed out due to internal (migration) or environmental transformations (NGC 4565 has an asymmetric warp and is interacting; van der Kruit 1979). Whether these arguments can be extended to low-mass galaxies is unclear. Galaxies with different masses may form thick disks through different paths (Comerón et al. 2012).

We have reported the discovery of a truncation linked to a SF threshold in the disk of an edge-on diffuse galaxy. The sharp SB drop-off is found at the same location in NIR, optical, NUV, and FUV bandpasses (Sect. 3.1). Moreover, it is detected at the same radius in both the thin and thick disks, the latter being defined from decomposition models of  $3.6 \mu\text{m}$  images by Comerón et al. (2018). This challenges thick disk formation models and gives rise to various interpretations. Comerón (2021) predict that the age of the youngest stars in thick discs is  $\sim 4 - 6$  Gyr for galaxies with a total stellar mass of  $\mathcal{M}_* \approx 10^9 \mathcal{M}_\odot$ . Thus, low-mass galaxies such as UGC 7321 may host relatively young thick disks whose SF threshold is preserved and similar to that of the thin disk. In this sense, our observations are likely a consequence of the pristine nature of UGC 7321 in terms of dynamics and SF, relative to giant spirals (Matthews et al. 1999). The low level of UV radiation detected in the region of the thick disk is likely associated with the emission from  $\text{H II}$  regions in the mid-plane of this super-thin galaxy. In fact, some UV clumps in the thin disk can have a full-width-at-half-maximum as large as  $10 - 15''$ .

The truncation in a thick disk can also result from both heating and radial and vertical migrations, despite the galaxy being isolated (Roškar et al. 2013). Thick disks can be made through embedded flares of mono-age stellar populations (Minchev et al. 2015). Moreover, simulations by Minchev et al. (2012) showed that secular evolution (no external perturbations) can form flared disks due to angular momentum redistribution caused by spirals or bars. This is consistent with the report of a flared disk in UGC 7321 by Sarkar & Jog (2019), where the used data probe the disk up to  $x = 2$  arcmin, while the flaring is predicted beyond this point, far out in the outskirts (the factor of  $\sim 2$  difference in their adopted distance with respect to our work is noted).

If such a flare exists, it should happen at a very low SB ( $\mu_{3.6\mu\text{m}}(\text{AB}) > 26 \text{ mag arcsec}^{-2}$ ), and its contribution to the thick disk fit would not be large. It is not noticeable from the images presented in Sect. 2. The fits of the outermost vertical cuts of  $3.6 \mu\text{m}$  SB performed by Comerón et al. (2018) indeed yielded  $\sim 20\%$  larger scale-heights, for both thin and thick disks, than those of the innermost cuts<sup>2</sup>. That is, the scale heights moderately increase with increasing axial distance. (Unfortunately, these outer fits did not fulfil the Comerón et al. quality criteria in

<sup>2</sup> Inner and outer vertical cuts refer to those averaged over axial ranges  $0.2R_{25} < x < 0.5R_{25}$  and  $0.5R_{25} < x < 0.8R_{25}$ , respectively, where  $R_{25}$  is the isophotal  $25 \text{ mag arcsec}^{-2}$  radius in the  $B$  band (for further details, see Comerón et al. 2012). For UGC 7321, inner and outer axial ranges correspond to roughly  $[3-7.5]$  kpc and  $[7.5-12.5]$  kpc, respectively.

the decompositions, but the thick disk component is also present in them.) We conclude that the outer parts of its thick disk may be biased by the light of a flared thin disk, but this effect should be negligible as the thick disk already dominates at  $3.6\ \mu\text{m}$  SB levels as high as  $\mu_{3.6}(\text{AB}) \approx 24\ \text{mag arcsec}^{-2}$  (Comerón et al. 2018).

Bars do play an important role in the redistribution of material throughout the disk of massive galaxies (e.g. Debattista et al. 2006; Díaz-García et al. 2016a); this is the case of NGC 4565, which hosts a prominent peanut-shaped bulge (Jarvis 1986). Bars are also more frequent than previously thought in low-mass galaxies (Díaz-García et al. 2016b). Pohlen et al. (2003) provided evidence for peanut-shaped outer isophotes in UGC 7321 from an  $R$ -band image. A bar in UGC 7321, as also inferred from the analysis of its H I position-velocity diagram (Uson & Matthews 2003), may also be responsible for its stellar migration (but see Ghosh & Jog 2014). Thus, UGC 7321's thick disk may be linked to bar-induced internal dynamics. Likewise, the outer reddening of UGC 7321 (colour  $U$ -shape; Fig. 2) is likely associated with SF thresholds followed by bar-driven outer migrations of stars, as in NGC 4565 (Martínez-Lombilla et al. 2019).

## 5. Conclusions

We have reported the discovery of an outer truncation in the SB profile of the diffuse ultra-thin edge-on galaxy UGC 7321 that is seen in UV (GALEX FUV and NUV), optical (DESI  $grz$ ), and NIR (*Spitzer*  $3.6\ \mu\text{m}$ ) images. The truncation, detected at the same radius in both the thin and thick disks, hints at similar or interconnected (migration) formation mechanisms for both components. The truncation occurs at a deprojected stellar surface density of  $1.5 \pm 0.5\ \mathcal{M}_{\odot} \text{pc}^{-2}$ , in agreement with the theoretical gas density thresholds for SF. The redder colours beyond the truncation are indicative of the radial migration of stars to the galaxy's outskirts. As UGC 7321 is isolated and has no strong signs of accretion, our findings are consistent with its thick disk and truncations being formed via internal mechanisms alone.

*Acknowledgements.* We thank the anonymous referee for a constructive and detailed report. This project has received funding from the European Union's Horizon 2020 research and innovation programme under the Marie Skłodowska-Curie grant agreement No 893673, from the State Research Agency (AEI-MCINN) of the Spanish Ministry of Science and Innovation under the grant "The structure and evolution of galaxies and their central regions" with reference PID2019-105602GB-I00/10.13039/501100011033, and under the grant "Thick discs, relics of the infancy of galaxies" with reference PID2020-113213GA-I00, and from IAC project P/300724, financed by the Ministry of Science and Innovation, through the State Budget and by the Canary Islands Department of Economy, Knowledge and Employment, through the Regional Budget of the Autonomous Community. S.C. is especially grateful to the Natural Sciences and Engineering Research Council of Canada, the Ontario Government, and Queen's University for support through various scholarships and grants. A.W. acknowledges support from the STFC [ST/S00615X/1]. J.H.K. acknowledges support from the ACIISI, Consejería de Economía, Conocimiento y Empleo del Gobierno de Canarias and the European Regional Development Fund (ERDF) under grant with reference PROID2021010044. J.R. acknowledges funding from University of La Laguna through the Margarita Salas Program from the Spanish Ministry of Universities ref. UNI/551/2021-May 26, and under the EU Next Generation. This research makes use of python (<http://www.python.org>) and IDL ([https://www.harrisgeospatial.com/docs/using\\_idl\\_home.html](https://www.harrisgeospatial.com/docs/using_idl_home.html)).

## References

Abadi, M. G., Navarro, J. F., Steinmetz, M., & Eke, V. R. 2003, *ApJ*, 597, 21  
 Arora, N., Stone, C., Courteau, S., & Jarrett, T. H. 2021, *MNRAS*, 505, 3135  
 Azzollini, R., Trujillo, I., & Beckman, J. E. 2008, *ApJ*, 679, L69  
 Bakos, J., Trujillo, I., & Pohlen, M. 2008, *ApJ*, 683, L103  
 Banerjee, A. & Jog, C. J. 2013, *MNRAS*, 431, 582

Banerjee, A., Matthews, L. D., & Jog, C. J. 2010, *New A*, 15, 89  
 Bizyaev, D. V., Kautsch, S. J., Sotnikov, N. Y., Reshetnikov, V. P., & Mosenkov, A. V. 2017, *MNRAS*, 465, 3784  
 Bosma, A. 2017, in *Astrophysics and Space Science Library*, Vol. 434, *Outskirts of Galaxies*, ed. J. H. Knapen, J. C. Lee, & A. Gil de Paz, 209  
 Bouquin, A. Y. K., Gil de Paz, A., Muñoz-Mateos, J. C., et al. 2018, *ApJS*, 234, 18  
 Brook, C. B., Kawata, D., Gibson, B. K., & Freeman, K. C. 2004, *ApJ*, 612, 894  
 Byun, Y. I., Freeman, K. C., & Kylafis, N. D. 1994, *ApJ*, 432, 114  
 Chamba, N., Trujillo, I., & Knapen, J. H. 2020, *A&A*, 633, L3  
 Comerón, S. 2021, *A&A*, 645, L13  
 Comerón, S., Elmegreen, B. G., Knapen, J. H., et al. 2011, *ApJ*, 741, 28  
 Comerón, S., Elmegreen, B. G., Salo, H., et al. 2012, *ApJ*, 759, 98  
 Comerón, S., Elmegreen, B. G., Salo, H., et al. 2014, *A&A*, 571, A58  
 Comerón, S., Salo, H., & Knapen, J. H. 2018, *A&A*, 610, A5  
 Courteau, S., Cappellari, M., de Jong, R. S., et al. 2014, *Reviews of Modern Physics*, 86, 47  
 Dahari, O. 1984, *AJ*, 89, 966  
 Dalcanton, J. J., Yoachim, P., & Bernstein, R. A. 2004, *ApJ*, 608, 189  
 de Jong, R. S., Seth, A. C., Radburn-Smith, D. J., et al. 2007, *ApJ*, 667, L49  
 Debattista, V. P., Mayer, L., Carollo, C. M., et al. 2006, *ApJ*, 645, 209  
 Debattista, V. P. & Sellwood, J. A. 1999, *ApJ*, 513, L107  
 Dey, A., Schlegel, D. J., Lang, D., et al. 2019, *AJ*, 157, 168  
 Díaz-García, S., Salo, H., & Laurikainen, E. 2016a, *A&A*, 596, A84  
 Díaz-García, S., Salo, H., Laurikainen, E., & Herrera-Endoqui, M. 2016b, *A&A*, 587, A160  
 Elmegreen, B. G. & Elmegreen, D. M. 2006, *ApJ*, 650, 644  
 Elmegreen, B. G., Elmegreen, D. M., Tompkins, B., & Jenks, L. G. 2017, *ApJ*, 847, 14  
 Erwin, P., Pohlen, M., & Beckman, J. E. 2008, *AJ*, 135, 20  
 Eskew, M., Zaritsky, D., & Meidt, S. 2012, *AJ*, 143, 139  
 Fazio, G. G., Hora, J. L., Allen, L. E., et al. 2004, *ApJS*, 154, 10  
 Fliri, J. & Trujillo, I. 2016, *MNRAS*, 456, 1359  
 Foyle, K., Courteau, S., & Thacker, R. J. 2008, *MNRAS*, 386, 1821  
 Freeman, K. C. 1970, *ApJ*, 160, 811  
 Ghosh, S. & Jog, C. J. 2014, *MNRAS*, 439, 929  
 Gilhuly, C., Hendel, D., Merritt, A., et al. 2020, *ApJ*, 897, 108  
 Hall, C., Courteau, S., Jarrett, T., et al. 2018, *ApJ*, 865, 154  
 Henkel, C., Javanmardi, B., Martínez-Delgado, D., Kroupa, P., & Teuwen, K. 2017, *A&A*, 603, A18  
 Hodges-Klucik, E., Cafmeyer, J., & Bregman, J. N. 2016, *ApJ*, 833, 58  
 Infante-Sainz, R., Trujillo, I., & Román, J. 2020, *MNRAS*, 491, 5317  
 Jadhav, Y. V. & Banerjee, A. 2019, *MNRAS*, 488, 547  
 Jarrett, T. H., Cohen, M., Masci, F., et al. 2011, *ApJ*, 735, 112  
 Jarvis, B. J. 1986, *AJ*, 91, 65  
 Karachentsev, I. D., Kudrya, Y. N., Karachentseva, V. E., & Mitronova, S. N. 2006, *Astrophysics*, 49, 450  
 Kennicutt, Robert C., J. 1989, *ApJ*, 344, 685  
 Kennicutt, Robert C., J. 1998, *ARA&A*, 36, 189  
 Laine, J., Laurikainen, E., Salo, H., et al. 2014, *MNRAS*, 441, 1992  
 Leroy, A. K., Walter, F., Brinks, E., et al. 2008, *AJ*, 136, 2782  
 Martin, C. L. & Kennicutt, Robert C., J. 2001, *ApJ*, 555, 301  
 Martín-Navarro, I., Bakos, J., Trujillo, I., et al. 2012, *MNRAS*, 427, 1102  
 Martínez-Lombilla, C. & Knapen, J. H. 2019, *A&A*, 629, A12  
 Martínez-Lombilla, C., Trujillo, I., & Knapen, J. H. 2019, *MNRAS*, 483, 664  
 Matthews, L. D. 2000, *AJ*, 120, 1764  
 Matthews, L. D., Gallagher, J. S., I., & van Driel, W. 1999, *AJ*, 118, 2751  
 Meidt, S. E., Schinnerer, E., Knapen, J. H., et al. 2012, *ApJ*, 744, 17  
 Minchev, I., Famaey, B., Quillen, A. C., et al. 2012, *A&A*, 548, A127  
 Minchev, I., Martig, M., Streich, D., et al. 2015, *ApJ*, 804, L9  
 Muñoz-Mateos, J. C., Sheth, K., Gil de Paz, A., et al. 2013, *ApJ*, 771, 59  
 Muñoz-Mateos, J. C., Sheth, K., Regan, M., et al. 2015, *ApJS*, 219, 3  
 Nasonova, O. G., de Freitas Pacheco, J. A., & Karachentsev, I. D. 2011, *A&A*, 532, A104  
 Pérez, I. 2004, *A&A*, 427, L17  
 Peters, S. P. C., van der Kruit, P. C., Knapen, J. H., et al. 2017, *MNRAS*, 470, 427  
 Pinna, F., Falcón-Barroso, J., Martig, M., et al. 2019, *A&A*, 623, A19  
 Pohlen, M., Balcells, M., Lütticke, R., & Dettmar, R. J. 2003, *A&A*, 409, 485  
 Pohlen, M. & Trujillo, I. 2006, *A&A*, 454, 759  
 Radburn-Smith, D. J., Roškar, R., Debattista, V. P., et al. 2012, *ApJ*, 753, 138  
 Roediger, J. C. & Courteau, S. 2015, *MNRAS*, 452, 3209  
 Roediger, J. C., Courteau, S., Sánchez-Blázquez, P., & McDonald, M. 2012, *ApJ*, 758, 41  
 Román, J., Trujillo, I., & Montes, M. 2020, *A&A*, 644, A42  
 Roškar, R., Debattista, V. P., & Loebman, S. R. 2013, *MNRAS*, 433, 976  
 Saintonge, A., Kauffmann, G., Wang, J., et al. 2011, *MNRAS*, 415, 61  
 Salo, H., Laurikainen, E., Laine, J., et al. 2015, *ApJS*, 219, 4  
 Sánchez Almeida, J. 2020, *MNRAS*, 495, 78  
 Sarker, S. & Jog, C. J. 2019, *A&A*, 628, A58

- Schaye, J. 2004, *ApJ*, 609, 667  
Schönrich, R. & Binney, J. 2009, *MNRAS*, 399, 1145  
Sheth, K., Regan, M., Hinz, J. L., et al. 2010, *PASP*, 122, 1397  
Springob, C. M., Haynes, M. P., Giovanelli, R., & Kent, B. R. 2005, *ApJS*, 160, 149  
Stone, C., Courteau, S., & Arora, N. 2021, *ApJ*, 912, 41  
Trujillo, I., Chamba, N., & Knapen, J. H. 2020, *MNRAS*, 493, 87  
Tully, R. B., Courtois, H. M., & Sorce, J. G. 2016, *AJ*, 152, 50  
Uson, J. M. & Matthews, L. D. 2003, *AJ*, 125, 2455  
van der Kruit, P. C. 1979, *A&AS*, 38, 15  
van der Kruit, P. C. 1987, *A&A*, 173, 59  
Verdes-Montenegro, L., Sulentic, J., Lisenfeld, U., et al. 2005, *A&A*, 436, 443  
Verstappen, J., Fritz, J., Baes, M., et al. 2013, *A&A*, 556, A54  
Villumsen, J. V. 1985, *ApJ*, 290, 75  
Watkins, A. E., Laine, J., Comerón, S., Janz, J., & Salo, H. 2019, *A&A*, 625, A36  
Watkins, A. E., Salo, H., Laurikainen, E., et al. 2022, *A&A*, 660, A69  
Werner, M. W., Roellig, T. L., Low, F. J., et al. 2004, *ApJS*, 154, 1  
Yoachim, P. & Dalcanton, J. J. 2006, *AJ*, 131, 226  
Zschaechner, L. K., Rand, R. J., Heald, G. H., Gentile, G., & Józsa, G. 2012, *ApJ*, 760, 37